Volume 1 | Number 1 | Jan 2013 | Pages 1–100

Nanoscale

www.rsc.org/nanoscale

Nanoscale

PAPER

TiO$_2$/CdSe Core-shell Nanofiber Film for Photoelectrochemical Hydrogen Generation

Ya liu, Liang Zhao, Mingtao Li,[*] and Liejin Guo

We report on a novel core-shell TiO$_2$/CdSe nanofiber photoanode for photoelectrochemical hydrogen generation. The core-shell nanofiber films, with hierarchical network structure, are prepared on fluorine-doped tin oxide coated substrates *via* electrospinning pyrolysis and chemical bath deposition. The hierarchical network structure shows significantly improved photoelectrochemical properties due, we believe, to more active sites for oxidation reaction and larger TiO$_2$/CdSe interface area for photogenerated charges separation. Synthesis details are discussed to provide a generic route for preparing other similar photoanodes in hierarchically network structure.

Introduction

Photoelectrochemical (PEC) hydrogen generation process is considered to be one of the most promising techniques to meet the energy shortage.[1] Numerous researches demonstrate the structure of photoanode has an important influence on the energy conversion efficiency.[2] Therefore, semiconductors with various nanostructures such as nanoparticle, nanoplate, nanorod, and nanotube are designed to promote energy conversion efficiency for hydrogen generation as the photoanodes.[3-9] Among them, one-dimensional structure attracts more and more attention due to the superior charge transport properties, few grain boundaries, and quick ion diffusion at the semiconductor-electrolyte interface.[8, 10]

As one of one-dimensional structures, ceramic nanofiber plays a vital role in various applications such as dye-sensitized solar cell,[11] fuel cell,[12] photodetector,[13] and hydrogen storage.[14] For PEC hydrogen generation, ceramic nanofiber can be used as an ideal framework and charge transport channel for catalyst in photoanode because of the exhibited features and properties such as one-dimensional morphology, high surface area, and hierarchical structure.[15, 16] Nanofiber, however, has seldom been researched on PEC application due to the limited preparation technology.

Finding a generic route for preparing photoanodes based nanofiber structure is very significant for further promoting the photoconversion efficiency in PEC application. Li *et al.* firstly reported a procedure based on electrospinning for generating ceramic nanofiber.[17] Uniformed TiO$_2$ nanofiber with network structure has been successfully fabricated in their work. Subsequently, Chuangchote *et al.* tested the photocatalyst properties for TiO$_2$ nanofiber, which, as well, was prepared based on electrospinning as well.[18] After calcined at 450 °C, the TiO$_2$ nanofiber showed higher activity than reference commercial TiO$_2$ nanoparticles. It is generally known that PEC hydrogen generation has a similar principle with photocatalyst in a particulate suspension system.[2] Thus, utilizing

electrospinning to prepare TiO$_2$ photoanode with network structure may achieve considerable PEC performance.

Except for the structure, it is also vital to select appropriate material. Although many semiconductors show PEC activity, preparing photoanode with single material could hardly solve the high charge carrier recombination rate and poor absorption of visible light.[19] While using narrow band gap semiconductors such as CdS,[20-22] CdSe,[23-26] and CdTe[27] to sensitize the wide band gap semiconductor has proved to be an effective approach to extend the optical absorption ability and hence enhance the PEC performance. Among those narrow band gap semiconductors, CdSe could absorb most of the visible light, and the energy bands of it match TiO$_2$ very well.[23-26, 28-30]
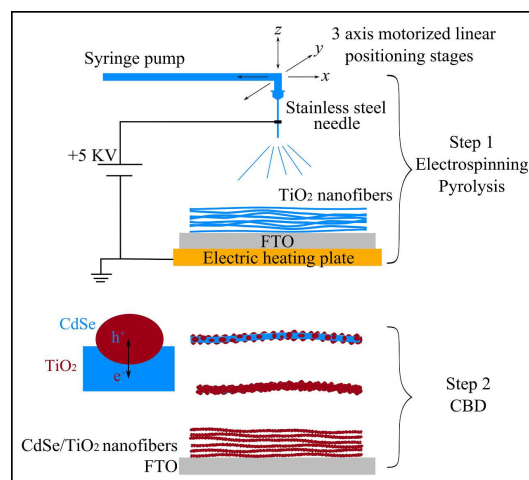

Fig. 1. Schematic illustration of the fabrication strategy for TiO$_2$/CdSe nanofiber films.

In this study, TiO$_2$/CdSe core-shell nanofiber films with a hierarchical network structure are prepared on fluorine-doped tin oxide coated substrates *via* electrospinning pyrolysis and chemical bath deposition (CBD). As one of the most

extensively studied materials in PEC application,[9, 31] TiO_2 was select as the framework and charge transport channel for photoanode. CdSe, as a narrow band gap energy semiconductor, was used to extend light absorption range. The stepwise band-edge structure within the interface combination between TiO_2 and CdSe can promote the electron-cavity separation efficiency.[23-25, 32] PEC measurements indicate that the illustrative photoanodes show pretty good photoconversion efficiency.

Experimental

Fabrication TiO_2/CdSe nanofiber films

TiO_2/CdSe nanofiber films were prepared by electrospinning pyrolysis and CBD approach which are shown in Fig. 1. TiO_2 nanofiber film was firstly deposited on fluorine-doped tin oxide (FTO) substrates *via* electrospinning pyrolysis. Before deposition, the substrates were ultrasonically pre-cleaned in acetone, de-ionized water, and ethanol 30 minutes respectively, and then dried with a stream of nitrogen. The spray solution was prepared by dissolving 0.15 g PVP (K90, Mw ≈ 1 300 000), 1.25 mmol tetrabutyl titanate (TBOT), and 0.125 mmol acetylacetone in 5 ml ethanol. After magnetically stirred for 6 hours, the as-prepared spray solution was pumped to the tip of a stainless steel needle (27 Gauge) by a syringe pump. The distance between the substrates and the tip of the needle was adjusted to 5 cm. The temperature of electric heating plate was slowly raised to 350 °C. During electrospinning pyrolysis, the flow rate was maintained at 0.5 ml per hours. The high direct current (DC) voltage was set at 5 KV, and the nozzle kept reciprocating scanning. Subsequently, the as-prepared PVP/TBOT nanofiber film was calcined at 500 °C for 3 hours to improve sample crystalline and remove organic residues in a muffle furnace.

CdSe particles were deposited on the surfaces of TiO_2 nanofibers by a CBD approach. Firstly, 0.02 mol of selenium powder was added into 100 mL of Na_2SO_3 aqueous solution (0.5 mol/L). Then this solution was maintained at 70 °C for 5 hours under nitrogen purge gas to achieve the fresh Na_2SeSO_3 solution. The Na_2SeSO_3 solution was used as the Se source for depositing CdSe particles during CBD. The CdSe precursor solution was prepared by dissolving KOH (0.505 g), nitrilotriacetic acid (0.57 g), $Cd(NO_3)_2$•$4H_2O$ (0.617 g), and Na_2SeSO_3 solution (10 mL) in 100 ml of de-ionized water. The prepared TiO_2 nanofiber films were put into above CdSe precursor solution and kept at a constant temperature of 70 °C for several hours. After the reaction, composite films were washed by de-ionized water and then dried with a stream of nitrogen for further tests.

Characterization

A JEOL JSM-7800F scanning electron microscope (SEM) and a FEI Tecnai G2 F30 transmission electron microscope (TEM) were used to characterize the morphology and structure of the films. The X-ray diffraction (XRD) analysis of the phase and crystal structure of the films was performed by an X'pert PRO diffractormeter (PANalytical, using Cu Kα irradiation (λ= 15.4184 nm)). Reflectance and transmittance spectra of the films was performed using a double-beam UV4100 UV-vis-NIR spectrophotometer equipment.

Photoelectrochemical measurements

PEC measurements were carried out in a three-electrode system. The films were used as the work electrode and installed onto a self-made electrode holder with the surface areas of 0.785 cm^2. A platinum foil was used as the counter electrode. A saturated calomel electrode Ag/AgCl (silver and silver chloride) was used as the reference electrode. An aqueous solution of 0.5 M Na_2SO_3 was used as the electrolyte. Photocurrent densities were measured by a CHI 760D scanning potentiostat (CH Instruments). The scanning rate was 10 mV/s, and the scanning direction was from low to high potential. A 500 W xenon lamp coupled with an AM1.5 filter was used as the light source. The light intensity was set at 100 mW/cm^2. The potential, against an Ag/AgCl reference, was converted to RHE (reversible hydrogen potential) potential using the formula $V_{RHE} = V_{Ag/AgCl} + 0.059pH + 0.1976V$, where V_{RHE} is a potential versus a reversible hydrogen potential, $V_{Ag/AgCl}$ is the potential versus Ag/AgCl electrode, and pH is the pH value of electrolyte.[33, 34]

Apart from the devices used in photocurrent densities measurement, a Newport monochromator 74126 and a quartz convex lens was used during IPCE measurement. The absolute intensity of the incident light was measured by a radiometer/photometer Model IL1400BL from International Light. Moreover, the PEC stability was measured in a sealed PEC cell with the surface areas of 3.14 cm^2. The current-time curve and H_2 evolution plot can be obtained at the same time. The light source was as same as the photocurrent densities measurement. Hydrogen evolved was detected by thermal conductivity detector (TCD) gas chromatograph, TDX-01 column, and Ar carrier gas.

Results and discussion

To obtain pure TiO_2 nanofiber, PVP/TBOT nanofiber must be thoroughly decomposed after or during electrospinning. When dispersive TiO_2 nanofiber was needed only, PVP/TBOT nanofiber was sprayed on a substrate at normal temperature and then thoroughly decomposed after further calcination.[17, 18] If PVP/TBOT nanofiber was sprayed on a FTO substrate at normal temperature, TiO_2 nanofiber would fall off from FTO because of the excessive shrink caused by decomposition. Thus, using heated substrate was studied for fabricating TiO_2 nanofiber film. Fortunately, the proper substrate temperature of 350 °C was found from a series of contrast experiments. PVP/TBOT nanofiber would be partially decomposed after ejecting from the needle and before reaching the FTO substrate due to the high temperature of the FTO substrates. The partial decomposition significantly reduced the shrink rate during further calcination. Crystalline TiO_2 nanofiber film was obtained after calcined in air at 500 °C for 3 hours.
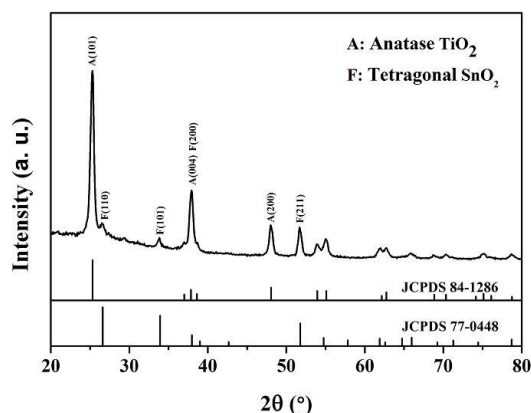

Fig. 2. XRD pattern of TiO_2 nanofiber film.

Fig. 2 presents XRD pattern of TiO_2 nanofiber film after calcined. Except for the characteristic diffraction peaks of FTO (standard card JCPDS 77-0448), some new peaks were found at 25.3º, 37.9º, and 48.0º. All new peaks were indexed to standard card JCPDS 84-1286 which corresponds to anatase-type TiO_2. This result indicated that TiO_2 nanofiber prepared in the present study has an anatase crystal structure and no any other secondary TiO_2 phase exits.
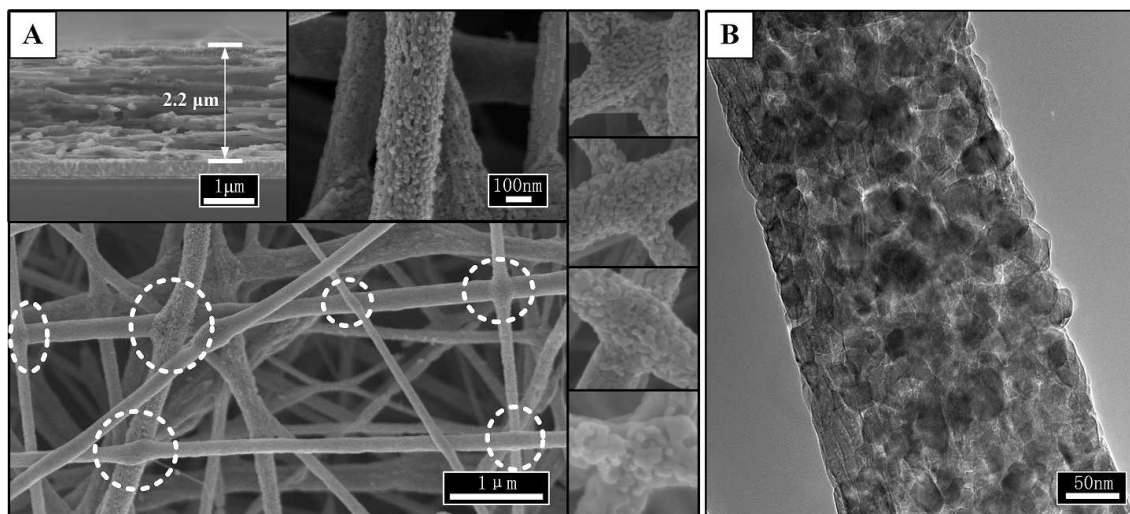

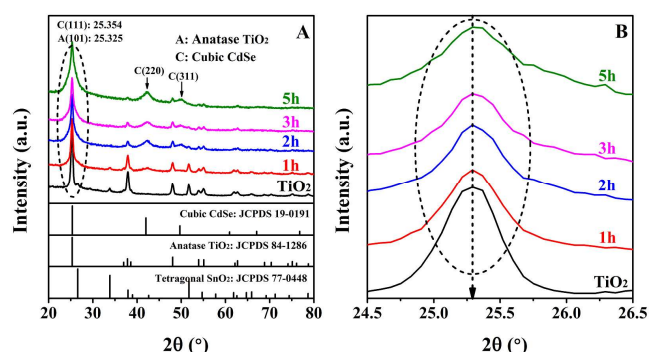Fig. 3. (A) SEM images and (B) TEM images of TiO_2 nanofiber film.

Fig. 4. (A) XRD patterns of TiO_2 and TiO_2/CdSe nanofiber films with different deposition time, and (B) detailed XRD patterns around 25.3º (circled area in (A)).
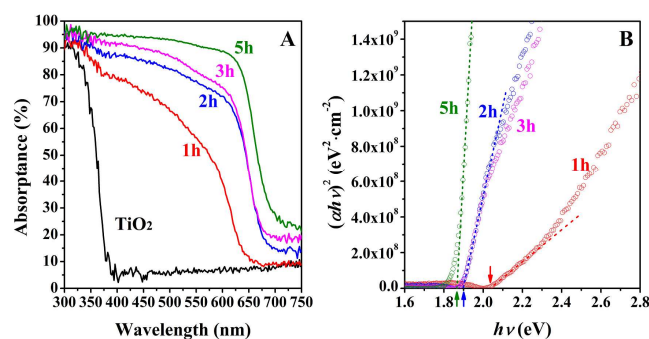

Fig. 5. (A) Spectral absorptance curves and (B) plot of $(\alpha h\nu)^2$ versus photon energy of TiO_2 and TiO_2/CdSe nanofiber films.

The morphology of TiO_2 nanofiber film was measured by SEM (as shown in Fig. 3A). TiO_2 nanofibers lay on FTO substrate and had a hierarchical network structure. The diameters of the nanofibers were between 20 nm and 200 nm. The thickness of the film was about 2.2 μm. Observed from the high magnification images, the nanofibers present a poriferous surface which can enlarge the specific surface area greatly. The crossing points (as shown in the white circle and insets of Fig. 3A) of nanofibers developed together to tight junctions. These tight junctions and nanofibers can form the transmission routes for charge carriers in PEC reaction. TEM image, shown in Fig. 3B, indicates that the TiO_2 nanofibers were made by scores of nanoparticles around a few tens of nanometers in diameter. These unique properties such as network structure, poriferous surface (large specific surface area), and tight junctions of the crossing points make this TiO_2 nanofiber film can be used as an ideal frame substrate to couple with other narrow band gap catalysts.

CdSe was selected as the visible light absorber to extend light absorption range and promote the efficiency of electron-cavity separation. The size and the loading amount which seriously affect the light absorption and charge carriers transfer can be controlled by deposition time.[30] Therefore, different deposition time was studied here to find the top-performing TiO_2/CdSe nanofiber film and reveal the PEC properties of the photoanode with hierarchical network structure. The deposition time was set at 1, 2, 3, and 5 hours respectively. The films with different CBD were described as 1h, 2h, 3h and 5h.

Fig. 4A introduces XRD patterns of TiO_2/CdSe nanofiber films with different deposition time. The block peaks at 2 theta of 42.1º and 49.7º can be indexed to (220), (311) crystal planes of cubic CdSe in standard card JCPDS 19-0191. However, the peaks of cubic CdSe (111) and anatase TiO_2 (101) surfaces were overlapped around 25.3º. It can be observed in Fig. 4B that this coupling peak broadens and shifts slightly to a higher angle as deposition time increase. Those appearances indicate the transformation of peaks from anatase (101) to cubic (111) surface. From these analysis results of XRD, it can be identified that CdSe was deposited on the films successfully. The ever-increasing intensities of cubic CdSe peaks reveal the amount of CdSe increased as the deposition time increased.

In general, it is a straightforward and useful way to characterize the optical properties of film by calculating its absorptance as 1 - transmittance - reflectance after measuring its spectral reflectance and transmittance.[35, 36] The absorptances

spectra of the films are displayed in Fig. 5A. Relative to TiO_2 the absorption regions of the composite samples obviously extended into the visible light region. The absorptance of the composite films increase as the deposition time increases. After deposited for 5 hours, the composite film could absorb light within the absorption edge sufficiently (more than 90 percent on average). It indicated that there is no need for a longer time deposition. Moreover, it is evident from Fig. 5A that the absorption edges of the composite films changed with the deposition time which indicated a band gap energy change of $CdSe$.[30] The optical band gap can be extracted from transmittance and reflectance spectra using Tauc plot method in equation[30, 37, 38]

$$\alpha h\nu \propto C(h\nu - E_g)^n \qquad (1)$$

Where α is the absorption coefficient, C is the photon energy dependent constant, $h\nu$ is photo energy, and E_g is band gap energy. Exponent n takes the values 1/2 for direct optical transitions and 2 for indirect optical transitions. In addition, absorption coefficient α can be expressed by the equation[39]

$$\alpha d = ln(T/(1 - R)^2) \qquad (2)$$

Where d, T and R represent film thickness, transmittance, and reflectance of the films respectively. Exponent n takes value 1/2 because numerous works and theoretical calculations suggest that cubic CdSe is direct optical transition materials.[40] Fig. 5B shows $(\alpha h\nu)^2$ versus photon energy plot. However, all of the band gaps achieved here were larger than that of bulk CdSe, which is 1.7 eV on account of the quantum confinement effect.[29] Furthermore, the optical band gaps of CdSe gradually decrease from 2.04 eV to 1.87 eV as the deposition time increases, except the nuance between 2 hours and 3 hours deposition. This diminution of band gaps suggests the size of CdSe might increase as the deposition time increases.[29, 30]
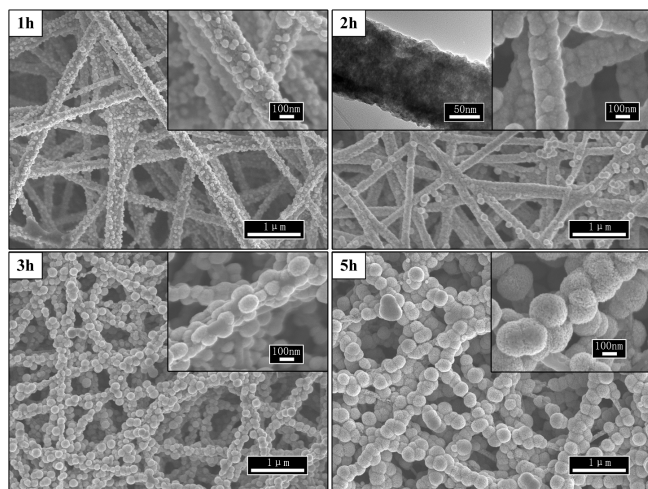

Fig. 6. SEM images of $TiO_2/CdSe$ nanofiber films with different deposition time, and TEM images (inset in 2h) of composite film with 2 hours deposition.

Fig. 6 shows the SEM images of the composite nanofiber films. After 1 hour deposition, TiO_2 nanofibers were studded with CdSe nanoparticles uniformly, and the diameters of CdSe nanoparticles were in a range of dozens of nanometer (according to1h in Fig. 6). As evident from the 2h in Fig. 6 that TiO_2 nanofibers were just completely enwrapped uniformly by CdSe nanoparticles. Besides, the inset TEM image in Fig. 6 verified that CdSe nanoparticles connected closely and tightly to TiO_2 nanofiber, and the core-shell nanofiber structure was obtained. However, when increased the deposition time

continually more than 3 hours, CdSe nanoparticles grew up to disorder big microspheres (displayed in 3h and 5h of Fig. 6). Meanwhile, the gaps between the nanofibers were notably diminished by CdSe particles.
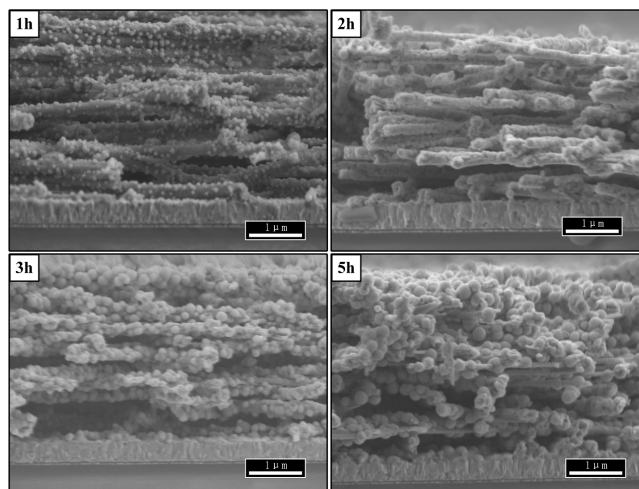

Fig. 7. Cross-sectional views of SEM images for $TiO_2/CdSe$ nanofiber films with different deposition time.

The cross-sectional views of the composite films are displayed in Fig. 7. When the deposition time was 1 or 2 hours, CdSe was uniformly deposited in vertical direction to the FTO plane (displayed in 1h and 2h of Fig. 7). This uniform deposition also demonstrates nanofibers in the inner layer can directly react with aqueous solution like the outer layer. From this, we can infer that, not only the outer layer of nanofibers network but also the inner layer of that can be involved directly in the PEC reaction. However, the longtime deposition would result in nonuniform growth of CdSe in the vertical direction (as indicated in 3h and 5h of Fig. 7). A possible explanation is that the diminished gaps between the nanofibers in the outer layer (displayed in Fig. 6) held back the reactants permeating through the nanofibers layer. Thus, we can also infer that for the longtime deposition films, the reaction between electrolyte and catalysis in the inner layer would be limited by lack of timely replenishing electrolyte in the PEC reaction.
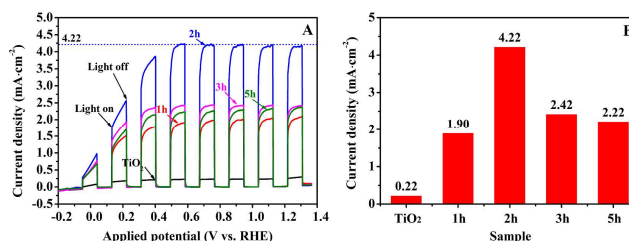

Fig. 8. (A) Current-potential curves under white light illumination and (B) photocurrents with an applied potential of -0.566 V (versus RHE) for TiO_2 and $TiO_2/CdSe$ nanofiber films.

By comparing above analyses of structure, optical absorption abilities, and morphology, it can be conjectured that although the longtime deposition promotes light absorption, it also extend the transmission distance of charge carriers and against the reaction between the electrolyte and catalysis in the inner layer. There must be an appropriate deposition time to achieve the best PEC performance. Fig. 8 compares the PEC

performance of TiO_2 and TiO_2/CdSe nanofiber films. All the composite films exhibited obvious enhancement of photocurrent densities than TiO_2 nanofiber film and reached saturation at potential above -0.566 V versus RHE. When deposition time was 2 hours, the highest saturated photocurrent density value was achieved at 4.22 mA/cm^{-2} with the applied potential of -0.566 V versus RHE. The highest saturated photocurrent density is almost 16 times more than that of the TiO_2 nanofiber film. Moreover, the photocurrent densities of films deposited more than 2 hours (3 hours and 5 hours) show seriously decrease. This result provides evidence of the above surmise, and the optimum deposition time is 2 hours.
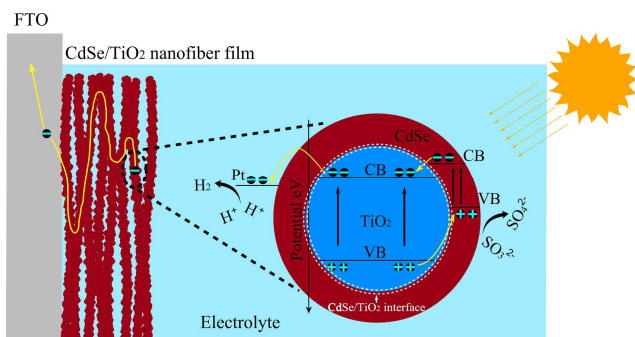

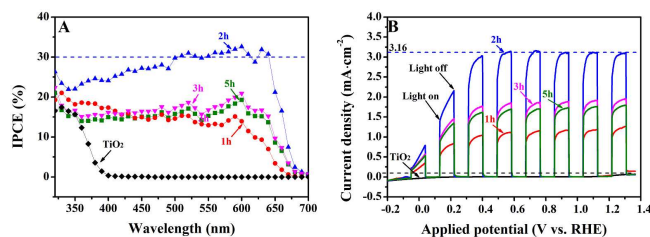Fig. 9. Sketch showing the nanostructure and charge-transfer processes for TiO_2/CdSe nanofiber film.

Fig. 10. (A) IPCE, and (B) visible light illuminated current-potential curves for TiO_2 and TiO_2/CdSe nanofiber films.

In order to describe the mechanism of electrode reaction better, the sketch of the nanostructure and charge-transfer processes for TiO_2/CdSe nanofiber film is displayed in Fig. 9. The hierarchical network structure makes TiO_2 nanofiber can absorb more CdSe nanoparticles than structures based on nanoparticle, nanorod, or nanotube. The poriferous surface on TiO_2 nanofiber (as shown in Fig. 3) obviously extended the area of the interface combined between anatase TiO_2 and cubic CdSe. A stepwise band-edge structure was built within such interface and could promote the electron-cavity separation efficiency.[23-25, 32] The electrons excited by light transfer through nanofibers and the crossing points in a roundabout way to reach FTO. When the deposition time was 2 hours, the procedure of CBD deposition revealed that all surface of core-shell nanofiber can be involved directly in the PEC reaction and provide plenty active sites for oxidation reaction. While increasing the deposition time over 2 hours, although the light absorption increased (as shown in Fig. 5), the long charge transmission distance and small gaps between nanofibers (as shown in Fig. 6) were the greater impacts that attenuated the photocurrent density.

The photocurrent density performance of all the films was also tested under monochromatic light and visible light illumination for further research on the PEC response to the light at various wavelengths. Comparing with the photocurrent

under white light, IPCE can better characterize the PEC performance because it has no connection with the light source in the measurement.[41] $IPCE_\lambda$ is the IPCE corresponded to the wavelength of the incident light is λ and can be calculated by the following equation[42]

$$IPCE_\lambda = (hc/e)(I_{ph,\lambda}/\lambda P_\lambda) \qquad (3)$$

Where h is the Plank's constant, c is the speed of light in vacuum, e is the elementary charge, $I_{ph,\lambda}$ represents the photocurrent density, P_λ is the power intensity of the incident monochromatic light. The IPCE plot is presented in Fig. 10A. Measurements were conducted in an aqueous 0.5 M Na_2SO_3 solution at applied potential of 0.766 V versus RHE. After deposited for 1 and 2 hours, the increased IPCE in UV range demonstrates the enhanced separation and transportation of photoexcited charge carriers. This enhancement was attributed to the stepwise band-edge structure in the interface combined between anatase TiO_2 and cubic CdSe. However, IPCE diminished after deposited for 3 and 5 hours due to the long charge transmission distance and small gaps between nanofibers. It is generally known that the solar energy in visible light range is much larger than that in UV range. Visible light must be the major contributor to photocurrent density for the composite films. The enhancement of IPCE in the visible light range was huge. The composite film deposited for 2 hours exhibits the best IPCE performance and the average IPCE in the visible part was around 30% while TiO_2 film displayed almost no response to visible light.

Fig. 10B shows current-potential curves under visible light illumination. A long-wave ($\lambda > 430$ nm) pass filter was used to shield UV light. The highest photocurrent density was 3.16 mA/cm^2 with the applied potential of -0.566 V versus RHE. Compared with the photocurrent density under the white light, it can be seen that the electric energy coming from visible light region contributed almost three quarters of that coming from the all-region. While photocurrent density measured for the bare TiO_2 film was negligible. These results are well consistent with the IPCE analysis.
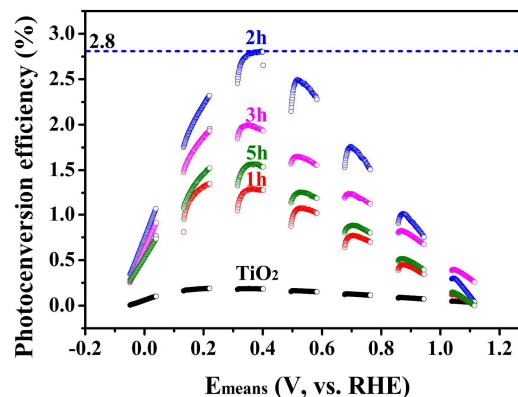

Fig. 11. Photoconversion efficiency for TiO_2 and TiO_2/CdSe nanofiber films.

The photoconversion efficiency (ε_{eff}), which corresponds to solar energy to chemical energy conversion efficiency in the presence of an external applied potential E_{app}, was also computed in this work and can be expressed as[43-45]

$$\% \ \varepsilon_{eff} = [j_p \ (E^0_{rev} - |E_{app}|) \times 100/(I_0)] \qquad (4)$$

Where j_p is the photocurrent density (mA/cm^2), E^0_{rev} is the standard state-reversible potential of 1.23 V for the water-splitting reaction, I_0 is the power density intensity of the

incident light (mW/cm^2), and $|E_{app}|$ is the absolute value of the applied potential Eapp which can be obtained as[43-45]

$$E_{app} = E_{meas} - E_{aoc} \quad (5)$$

Where E_{meas} is the electrode potential (versus Ag/AgCl) at which j_p was measured, and E_{aoc} is the electrode potential at open circuit condition under the same light illumination and in the same electrolyte solution at which j_p was measured. Fig. 11 displays the photoconversion efficiency of all the films. The composite film deposited CdSe for 2 hours gives the highest photoconversion efficiency value of 2.8% with the applied potential of -0.366 V versus RHE.

Some previous works have been reported to fabricate TiO$_2$/CdSe photoanodes used in the similarity application system. Kongkanand *et al.* used different-sized CdSe quantum dots to couple with TiO$_2$ nanoparticle or nanotube films.[24] The

maximum IPCE was 35% for particulate TiO$_2$ and 45% for tubular TiO$_2$ morphology. The CdSe/TiO$_2$ nanotube film obtained the maximum power-conversion efficiency of nearly 1%. Afterwards, Bang and co-works sensitized rutile TiO$_2$ nanorod array with CdSe and utilized as a photoanode for solar cells.[25] The maximum IPCE of the CdSe/TiO$_2$ nanorod electrodes was nearly 25%. Moreover, Liang *et al. in situ* electrodeposited CdSe clusters on TiO$_2$ nanotube.[26] The maximum photocurrent density was nearly 2 mA/cm^{-2} with the applied potential of 0 V versus Ag/AgCl under visible light illumination ($\lambda > 430$ nm) in 1 M NaOH solution containing 1 M Na$_2$S and 1 M S. Compared with nanoparticle,[23, 28] nanotube,[24, 26] and nanorod[25] based photoanodes, the nanofiber based one in this work exhibits better PEC performance.
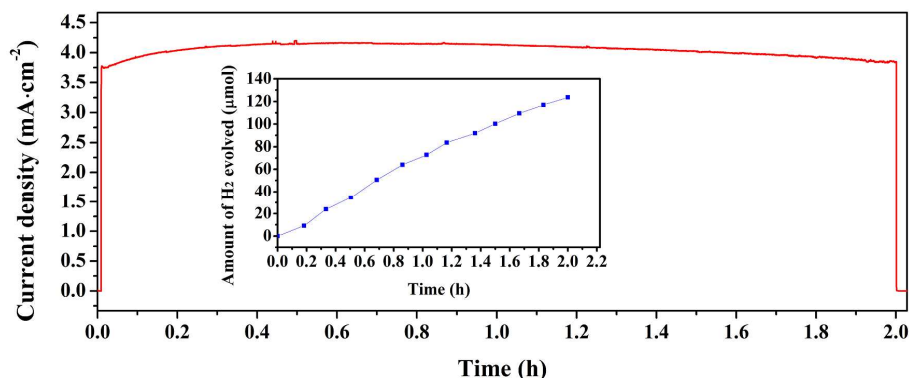

Fig. 12. Current-time curve at a 0.766 V vs. RHE for TiO$_2$/CdSe nanofiber film with 2 hours deposition. Inset shows the H$_2$ evolution plot.
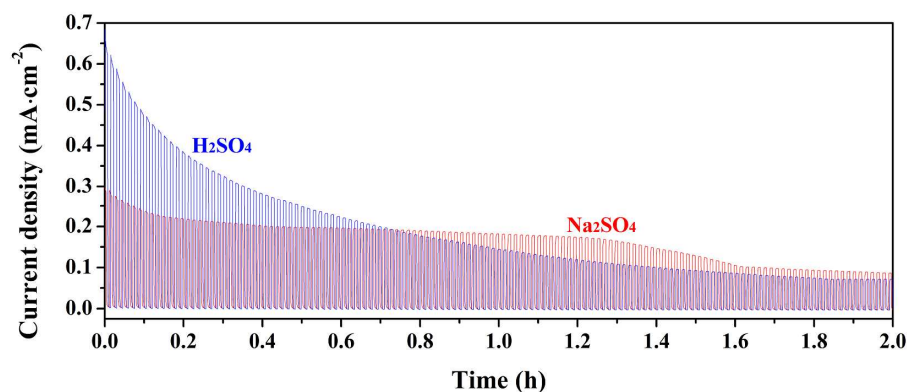

Fig. 13. Current-time curves for TiO$_2$/CdSe nanofiber film with chopped light source in Na$_2$SO$_4$ (0.5 M) and H$_2$SO$_4$ (0.1 M) electrolytes.

Photocorrosion is regarded as the main reason that causing the poor stability of photoanodes, especially the metal sulfides and selenides.[9] Although photocorrosion cannot be avoided, economic results can still be achieved by weakening the photocorrosion. In this study, the sacrificial electrolyte (Na$_2$SO$_3$) was used to prevent photocorrosion of the core-shell TiO$_2$/CdSe nanofiber structure. The PEC stability measurements were carried out in a sealed PEC cell. The current-time curve and H$_2$ evolution plot can be obtained at the same time. The applied potential was set at 0.766 V vs. RHE. As illustrated in Fig. 12, the highest photocurrent density was achieved after half an hour irradiation. The photocurrent density decreased about 5.2% per hour after 1 hour irradiation. Besides the insert plot in Fig. 12 indicates that TiO$_2$/CdSe

nanofiber film shows the ability for PEC H$_2$ production (61.78 µmol/h).

In this PEC reaction system, electrons unite with H$^+$ to obtain H$_2$ from water, and holes unite with SO$_3^{2-}$ to obtain SO$_4^{2-}$. Photocorrosion takes place only when the ions in solution are insufficient to cope with all the photogenerated holes.[46] If there is no SO$_3^{2-}$ to capture holes, OH$^-$ was inadequate to cope with all the photogenerated holes on CdSe/electrolyte interface. Thus Se^{2-} in photoanode will probably react with holes. For demonstrating this statement, additional PEC stability measurements were conductor in electrolytes of Na$_2$S$_2$O$_4$ (0.5M), and H$_2$SO$_4$ (0.1M). Fig. 13 shows current-time curves for TiO$_2$/CdSe nanofiber film with chopped light source. Low photocurrent densities and poor stability were displayed in

Na_2SO_4 and H_2SO_4 electrolytes compared with in Na_2SO_3. The low initial photocurrent densities may be attributed to the high valence band of CdSe which makes holes harder to cope with OH^- than SO_4^{2-}. The incessant reaction between holes and Se^{2-} seriously damaged the PEC stability of photoanode. Using sacrificial electrolyte (Na_2SO_3), thereby, is a reasonable way to achieve better economic results.

Conclusions

In summary, we successfully fabricated one-dimensional TiO_2/CdSe core-shell nanofiber films on fluorine-doped tin oxide coated substrates *via* electrospinning pyrolysis and chemical bath deposition. The film was based on a hierarchical network structure which was built by electrospinning pyrolysis. The poriferous surface of TiO_2 nanofiber and hierarchical network structure enabled the composite film can absorb more CdSe nanoparticles and have larger TiO_2/CdSe interface area than other structure based films such as nanoparticle,[23, 28] nanotube,[24, 26] and nanorod.[25] The procedure of CBD deposition revealed that all surface of core-shell nanofiber can be involved directly in the PEC reaction and provide plenty active sites for oxidation reaction. Series PEC tests demonstrated the hierarchical network structure has potential for improving PEC hydrogen generation efficiencies. PEC measurements of illustrative films show the highest photoconversion efficiency is 2.8% with the saturated photocurrent density of 4.22 mA/cm^{-2} with the applied potential of -0.566 V versus RHE. The highest IPCE was around 30% corresponding to the highest photocurrent densities of 3.16mA/cm^2 under visible light illumination. The PEC stability measurements show that the TiO_2/CdSe nanofiber film has the ability for PEC H_2 production (61.78 μmol/h). Although TiO_2 was selected in the present work, electrospinning pyrolysis is a versatile route to prepare oxides like ZnO, Fe_2O_3, WO_3, and SnO_2. This work described here could be extended to provide a generic route for preparing other similar photoanodes in hierarchically network structure for PEC application.

Acknowledgements

Notes and references

*Corresponding author: M. Li.

International Research Center for Renewable Energy (IRCRE), State Key Laboratory of Multiphase Flow in Power Engineering (MFPE), Xi'an Jiaotong University (XJTU), 28 West Xianning Road, Xi'an, Shaanxi 710049, P. R. China. E-mail: mingtao@mail.xjtu.edu.cn

1. A. Fujishima, *Nature*, 1972, 238, 37-38.
2. A. L. Linsebigler, G. Lu and J. T. Yates Jr, *Chemical Reviews*, 1995, 95, 735-758.
3. R. Solarska, C. Santato, C. Jorand-Sartoretti, M. Ulmann and J. Augustynski, *Journal of Applied Electrochemistry*, 2005, 35, 715-721.
4. M. Zukalova, A. Zukal, L. Kavan, M. K. Nazeeruddin, P. Liska and M. Grätzel, Nano Letters, 2005, 5, 1789-1792.
5. B. Liu, A. Khare and E. S. Aydil, *Chemical Communications*, 2012, 48, 8565-8567.
6. X. Feng, K. Shankar, O. K. Varghese, M. Paulose, T. J. Latempa and C. A. Grimes, *Nano Letters*, 2008, 8, 3781-3786.
7. J. H. Park, S. Kim and A. J. Bard, *Nano Letters*, 2006, 6, 24-28.
8. G. K. Mor, K. Shankar, M. Paulose, O. K. Varghese and C. A. Grimes, *Nano Letters*, 2006, 6, 215-218.
9. X. Chen, S. Shen, L. Guo and S. S. Mao, *Chemical Reviews*, 2010, 110, 6503-6570.
10. K. Zhu, N. R. Neale, A. Miedaner and A. J. Frank, *Nano Letters*, 2007, 7, 69-74.
11. L. Yang and W. W. F. Leung, *Advanced Materials*, 2011, 23, 4559-4562.
12. H.-J. Liu, X.-M. Wang, W.-J. Cui, Y.-Q. Dou, D.-Y. Zhao and Y.-Y. Xia, *Journal of Materials Chemistry*, 2010, 20, 4223-4230.
13. H. Wu, Y. Sun, D. Lin, R. Zhang, C. Zhang and W. Pan, *Advanced Materials*, 2009, 21, 227-231.
14. D. J. Browning, M. L. Gerrard, J. B. Lakeman, I. M. Mellor, R. J. Mortimer and M. C. Turpin, *Nano Letters*, 2002, 2, 201-205.
15. D. Li and Y. Xia, *Advanced materials*, 2004, 16, 1151-1170.
16. Y. Dai, W. Liu, E. Formo, Y. Sun and Y. Xia, *Polymers for Advanced Technologies*, 2011, 22, 326-338.
17. D. Li and Y. Xia, *Nano Letters*, 2003, 3, 555-560.
18. S. Chuangchote, J. Jitputti, T. Sagawa and S. Yoshikawa, *ACS Applied Materials & Interfaces*, 2009, 1, 1140-1143.
19. J. Su, L. Guo, N. Bao and C. A. Grimes, *Nano Letters*, 2011, 11, 1928-1933.
20. H. Wang, Y. Bai, H. Zhang, Z. Zhang, J. Li and L. Guo, *Journal of Physical Chemistry C*, 2010, 114, 16451-16455.
21. W.-T. Sun, Y. Yu, H.-Y. Pan, X.-F. Gao, Q. Chen and L.-M. Peng, *Journal of the American Chemical Society*, 2008, 130, 1124-1125.
22. Y. Liu, J. Jiang, Q. Xu, M. Li and L. Guo, *Materials Research Bulletin*, 2013, 48, 4548-4554.
23. I. Robel, V. Subramanian, M. Kuno and P. V. Kamat, *Journal of the American Chemical Society*, 2006, 128, 2385-2393.
24. A. Kongkanand, K. Tvrdy, K. Takechi, M. Kuno and P. V. Kamat, *Journal of the American Chemical Society*, 2008, 130, 4007-4015.
25. J. H. Bang and P. V. Kamat, *Advanced Functional Materials*, 2010, 20, 1970-1976.
26. Y. Liang, B. Kong, A. Zhu, Z. Wang and Y. Tian, *Chemical Communications*, 2012, 48, 245-247.
27. X.-F. Gao, H.-B. Li, W.-T. Sun, Q. Chen, F.-Q. Tang and L.-M. Peng, *Journal of Physical Chemistry C*, 2009, 113, 7531-7535.
28. N. Guijarro, T. Lana-Villarreal, I. Mora-Seró, J. Bisquert and R. Gómez, *Journal of Physical Chemistry C*, 2009, 113, 4208-4214.
29. A. M. Smith and S. Nie, *Accounts of Chemical Research*, 2009, 43, 190-200.
30. J.-W. Lee, J.-H. Im and N.-G. Park, *Nanoscale*, 2012, 4, 6642-6648.
31. X. Chen and S. S. Mao, *Chemical Reviews*, 2007, 107, 2891-2959.
32. J. Hensel, G. Wang, Y. Li and J. Z. Zhang, *Nano Letters*, 2010, 10, 478-483.
33. W. Luo, Z. Yang, Z. Li, J. Zhang, J. Liu, Z. Zhao, Z. Wang, S. Yan, T. Yu and Z. Zou, Energy & Environmental Science, 2011, 4, 4046-4051.
34. A. Kay, I. Cesar and M. Grätzel, Journal of the American Chemical Society, 2006, 128, 15714-15721.

35. I. S. Cho, Z. Chen, A. J. Forman, D. R. Kim, P. M. Rao, T. F. Jaramillo and X. Zheng, *Nano Letters*, 2011, 11, 4978-4984.

36. R. Levinson, P. Berdahl and H. Akbari, *Solar Energy Materials and Solar Cells*, 2005, 89, 319-349.

37. G. Zhu, L. Pan, T. Xu and Z. Sun, *ACS Applied Materials & Interfaces*, 2011, 3, 3146-3151.

38. M. A. Hossain, J. R. Jennings, C. Shen, J. H. Pan, Z. Y. Koh, N. Mathews and Q. Wang, *Journal of Materials Chemistry*, 2012, 22, 16235-16242.

39. R. Bhattacharya, *Journal of the Electrochemical Society*, 1983, 130, 2040-2042.

40. S. Ninomiya and S. Adachi, *Journal of Applied Physics*, 1995, 78, 4681-4689.

41. G. Wang, H. Wang, Y. Ling, Y. Tang, X. Yang, R. C. Fitzmorris, C. Wang, J. Z. Zhang and Y. Li, *Nano Letters*, 2011, 11, 3026-3033.

42. G. Wang, X. Yang, F. Qian, J. Z. Zhang and Y. Li, *Nano Letters*, 2010, 10, 1088-1092.

43. S. U. Khan, M. Al-Shahry and W. B. Ingler, *Science*, 2002, 297, 2243-2245.

44. J. Jiang, M. Wang, L. Ma, Q. Chen and L. Guo, *International Journal of Hydrogen Energy*, 2013, 38, 13077-13083.

45. M. Wang, J. Jiang, J. Shi and L. Guo, *ACS applied materials & interfaces*, 2013, 5, 4021-4025.

46. A. Heller, *Accounts of Chemical Research*, 1981, 14, 154-162.

Nanoscale Accepted Manuscript